Rock Mech Rock Eng (2017) 50:341–352
DOI 10.1007/s00603-016-1083-0

ORIGINAL PAPER

A New Rock Strength Criterion from Microcracking Mechanisms Which Provides Theoretical Evidence of Hybrid Failure

Qi-Zhi Zhu[1,2]

Received: 31 January 2016 / Accepted: 5 September 2016 / Published online: 17 October 2016

Abstract A proper criterion describing when material fails is essential for deep understanding and constitutive modeling of rock damage and failure by microcracking. Physically, such a criterion should be the global effect of local mechanical response and microstructure evolution inside the material. This paper aims at deriving a new mechanisms-based failure criterion for brittle rocks, based on micromechanical unilateral damage-friction coupling analyses rather than on the basic results from the classical linear elastic fracture mechanics. The failure functions respectively describing three failure modes (purely tensile mode, tensile-shear mode as well as compressive-shear mode) are achieved in a unified upscaling framework and illustrated in the Mohr plane and also in the plane of principal stresses. The strength envelope is proved to be continuous and smooth with a compressive to tensile strength ratio dependent on material properties. Comparisons with experimental data are finally carried out. By this work, we also provide a theoretical evidence on the hybrid failure and the smooth transition from tensile failure to compressive-shear failure.

Keywords Failure criterion · Micromechanics · Damage and friction coupling · Unilateral effects · Penny-shaped cracks · Brittle rocks

✉ Qi-Zhi Zhu
qizhi.zhu@gmail.com

[1] College of Civil and Transportation Engineering, Hohai University, Nanjing, China

[2] Key Laboratory of Ministry of Education for Geomechanics and Embankment Engineering, Hohai University, Nanjing, China

1 Introduction

Brittle rocks, either in their natural state or subjected to external loads, contain a large number of randomly oriented and distributed microcracks. In tension, these cracks are mostly open and will grow in response to locally concentrated stresses particularly at the tips. In that event, crack growth usually experiences an unstable stage toward a brittle failure. However, under increasing compressive stresses, nonlinear mechanical behaviors of the material are essentially governed by local coupling between friction-induced inelastic deformation and cracking-related damage evolution. Proper account of the unilateral effects and damage-friction coupling allows to explain and model lots of nonlinear mechanical phenomena usually observed at laboratory.

Theoretical prediction of macroscopic fracture stresses (strength) has been of great interest in mechanics and engineering science. For quasi-brittle microcracked rocks, the final failure is mainly attributed to damage cumulation due to crack growth. In the literature, various efforts have been made to predict material failure. Firstly, empirical attempts were devoted to setting up failure criteria based on experimental results. We can mention among others the well-known Mohr–Coulomb criterion, the Drucker–Prager criterion (Drucker and Prager 1952) and the Hoek–Brown criterion (Hoek and Brown 1980). However, these criteria are nearly based on mathematically empirical approaches. Starting from experimental values of failure stresses obtained from various loading paths (uniaxial tension and compression, conventional triaxial compression, true triaxial compression, direct shear test, Brazilian indirect tension test, etc.), one tried to determine a reduced form of mathematical criteria which are generally functions of stress invariants and material symmetry properties.

Therefore, strength prediction in such a way is completely separated from deformation analysis. Moreover, although capable of defining limiting conditions on failure stresses, these criteria concerned and told very little about physical mechanisms behind macroscopic phenomena as well as specific microstructure evolution closely related to potential failure modes for a given loading path. In particular, the transition between different failure modes, which has been experimentally evidenced by Ramsey and Chester (2004), has never been properly theoretically investigated. Because of the lack of consistent framework, the empirically obtained failure envelopes are often not smooth.

The Griffith failure theory proposed nearly a century ago remains up to now the cornerstone of studying initiation and propagation of a single crack. In his pioneering works, Griffith (1921, 1924) regarded initial cracks as the governing factor of brittle failure and then predicted the tensile strength by investigating the stress state at the tips of flat elliptical cracks. This theory succeeded to a large extent in incorporating material microstructure (cracks) into failure prediction. Later, the Griffith failure theory was extended to various aspects; for example, the extension to penny-shaped cracks (Keer 1966; Margolin 1984), the contributions for brittle fracture under compressive or shear stresses (McClintock and Walsh 1962; Hoek and Bieniawski 1965; Wang and Shrive 1993), the works for Griffith failure in three dimensions (Sack 1946; Kassir and Sih 1967; Hatzitrifon and Gdoutos 1988), the work by Brace (1960) to take into account pore pressure effect, just mention the representative ones. Comparisons of the Griffith theory with other well-known failure criteria have also been performed (Clausing 1959; Brace and Bombolakis 1963; Hoek and Martin 2014). It is worth noticing that in view of the importance of the Griffith theory, Patersson and Wong (2010) included in their book a whole chapter on this topic.

In the Mohr plane, the original Griffith failure function takes the form

$$\tau^2 + 4\sigma_t\sigma_n - 4\sigma_t^2 = 0 \tag{1}$$

with τ, σ_n and σ_t representing the norm of the shear stress vector, the normal stress and the tensile strength, respectively. As have been commented by McClintock and Walsh (1962), the criterion (1) presents some obvious deficiencies in predicting compressive strength, arising from the smaller increase in compressive strength as the confining pressure increases. Moreover, the predicted ratio of compressive strength to tensile strength is fixed at eight, but this ratio is found in experiment to vary for different rocks. In order to amend the discrepancy between theoretical predictions by the Griffith criterion and experimental observations, McClintock and Walsh (1962) made their own contributions by accounting for contact conditions and frictional sliding for closed cracks under local normal compression. To be definite, when $\sigma_n < 0$, the Griffith failure condition is modified as

$$\tau + \alpha\sigma_n - 2\sigma_t = 0 \tag{2}$$

where α is the coefficient of friction of crack surfaces. When $\sigma_n > 0$, the Griffith failure function was assumed to be still valid. It is worthy emphasizing that for the modified failure criterion, although the two parts always intersect at the τ-axis, its smoothness takes place only in the particular case where $\alpha = 1$, implying a mathematical inconsistency in this modification.

A criterion describing when material fails is essential, but still far from a complete constitutive modeling of mechanical behaviors of the material. Given a single strength criterion, there is still a need to incorporate into it evolution laws of both crack growth and inelastic strain and to introduce into it a hardening/softening function for achieving a complete material response. Differing greatly from the above common process, Zhu (2016) recently realized strength prediction in combination with deformation analysis for brittle rocks where use has been made of an upscaling method but under isotropic assumptions upon both inelastic strain and damage. As a further extension along the line, the present paper is devoted to setting up a new strength criterion from microcracking mechanisms via a well-developed micromechanics-based anisotropic unilateral damage-friction coupling model (Pensée et al. 2002; Zhu et al. 2008a, b, 2016; Zhu and Shao 2015). The closed-form failure functions are the inherent consequence of a combined unilateral damage/friction process. Not only the purely tensile failure mode but also the tensile-shear failure mode and the compressive-shear failure mode which may present in microcracked rocks are taken into account in a unified and consistent framework. The new criterion offers an enrichment to the original Griffith failure function and also to its modified version at least on three critical aspects: (1) in compression regime, it arises from a local Coulomb-type friction criterion in combination with a strain energy release rate-based damage criterion, both formulated on micro scale. Friction effect is thus taken into account in a proper way; (2) theoretical demonstration for the hybrid failure mode as well as the transition from the tensile failure mode to the compressive-shear failure mode; (3) the smoothness at the transition from the tensile to compressive-shear failure mode is ensured theoretically.

2 Constitutive Equations of the Matrix–Cracks System

This section briefly presents the micromechanics-based unilateral damage formulations, relying on which we will derive failure functions for microcracked brittle rocks.

2.1 System Free Energy

Focus here is put on brittle rocks whose matrix phase is weakened by a large number of randomly oriented and distributed penny-shaped microcracks. As usually performed in multiscale analyses, we extract a representative elementary volume (REV), which occupies a geometric domain Ω and has external boundary surface $\partial\Omega$. In this matrix–cracks system, the solid phase is assumed to be isotropic and linearly elastic with stiffness tensor $\mathbb{C}$. To facilitate mathematical formulations, microcracks with the same normal is put into a family. Geometrically, a family of penny-shaped cracks can be characterized by its normal vector $\boldsymbol{n}$, mean surface radius a and its half-opening c. The corresponding volume fraction ϕ^c is then given by $\phi^c = \frac{4}{3}\pi a^2 c\mathcal{N} = \frac{4}{3}\pi\varsigma d$ with $\varsigma = c/a$ being crack aspect ratio and $\mathcal{N}$ the number of cracks per unit volume. For each crack family, the dimensionless crack density parameter $d = \mathcal{N}a^3$ is taken as internal damage variable.

Microcracks in a family could be either open or closed. Therefore, we may envisage any open/closure combination of all considered representative crack families. We propose here to apply the Mori-Tanaka homogenization scheme (Mori and Tanaka 1973) to the matrix—(penny-shaped) cracks system. On the one hand, for simple matrix–cracks configurations, this scheme can produce the same results as those in the linear elastic fracture mechanics (Kachanov 1992; Benveniste 1986); on the other hand, the effective compliance predicted by this scheme is of linear form, which can facilitate significantly constitutive formulations. The Gibbs free energy of the REV described above takes the following general form (Zhu and Shao 2015)

$$\psi = \frac{1}{2}\boldsymbol{\sigma} : \mathbb{S}^{\text{hom}} : \boldsymbol{\sigma} + \boldsymbol{\sigma} : \sum_{j=1}^{n_c} \boldsymbol{\epsilon}^{c,j} - \sum_{j=1}^{n_c} \frac{1}{2d^j} \boldsymbol{\epsilon}^{c,j} : \mathbb{C}^{n,j} : \boldsymbol{\epsilon}^{c,j} \tag{3}$$

where $\mathbb{S}^{\text{hom}} = \mathbb{S} + \sum_{r=1}^{n_o} d^r \mathbb{S}^{n,r}$ is the effective compliance tensor with $\mathbb{S} = \mathbb{C}^{-1}$ being the compliance tensor of the matrix, $\boldsymbol{\sigma}$ is the macroscopic stress tensor; n_o and n_c represent the family number of open cracks and that of closed cracks, respectively; $\boldsymbol{\epsilon}^{c,j}$ denotes the local inelastic strain related to displacement discontinuities across the surfaces of closed cracks in the jth family. By using the fourth-order orientation-dependent operators $T_{ijkl} = \frac{1}{2}\left(n_i n_k \delta_{jl} + n_i n_l \delta_{jk} + n_j n_k \delta_{il} + n_j n_l \delta_{ik} - 4n_i n_j n_k n_l\right)$ and $N_{ijkl} = n_i n_j n_k n_l$, the fourth-order modulus tensor $\mathbb{C}^n$ and its pseudo-inverse $\mathbb{S}^n$ are given by

$$\mathbb{C}^n = c_n \mathbb{N} + c_t \mathbb{T}, \quad \mathbb{S}^n = \frac{1}{c_n}\mathbb{N} + \frac{1}{c_t}\mathbb{T}. \tag{4}$$

For penny-shaped cracks, c_n and c_t are two constants only function of the Young's modulus E and the Poisson's ratio v of the matrix, such that $c_n = 3E/16(1-v^2)$ and $c_t = (2-v)c_n$ (Kachanov 1992).

2.2 State Equations

The constitutive model based on the linear homogenization method is formulated within the framework of irreversible thermodynamics with internal variables. From Eq. (3) are derived the macroscopic strain

$$\boldsymbol{\varepsilon} = \frac{\partial\psi}{\partial\boldsymbol{\sigma}} = \mathbb{S}^{\text{hom}} : \boldsymbol{\sigma} + \sum_{j=1}^{n_c} \boldsymbol{\epsilon}^{c,j} \tag{5}$$

and the thermodynamic force associated with the local inelastic strain $\boldsymbol{\epsilon}^c$

$$\boldsymbol{\sigma}^c = \frac{\partial\psi}{\partial\boldsymbol{\epsilon}^c} = \boldsymbol{\sigma} - \frac{1}{d}\mathbb{C}^n : \boldsymbol{\epsilon}^c \tag{6}$$

$\boldsymbol{\sigma}^c$ is physically interpreted as the local stress acting on microcracks. Its normal part σ_n^c and tangential part $\boldsymbol{\tau}^c$ are obtained by projecting the stress vector $(\boldsymbol{\sigma}^c \cdot \boldsymbol{n})$ onto the normal direction and crack plane, respectively

$$\sigma_n^c = \boldsymbol{n} \cdot \boldsymbol{\sigma}^c \cdot \boldsymbol{n}, \quad \boldsymbol{\tau}^c = \boldsymbol{\sigma}^c \cdot \boldsymbol{n} \cdot (\boldsymbol{\delta} - \boldsymbol{n} \otimes \boldsymbol{n}), \tag{7}$$

or in a more explicit form

$$\sigma_n^c = \sigma_n - \frac{c_n}{d}\boldsymbol{\epsilon}^c : (\boldsymbol{n} \otimes \boldsymbol{n}), \quad \boldsymbol{\tau}^c = \boldsymbol{\tau} - \frac{c_t}{d}\boldsymbol{\epsilon}^c \cdot \boldsymbol{n} \cdot (\boldsymbol{\delta} - \boldsymbol{n} \otimes \boldsymbol{n}) \tag{8}$$

with $\sigma_n = \boldsymbol{n} \cdot \boldsymbol{\sigma} \cdot \boldsymbol{n}$ and $\boldsymbol{\tau} = \boldsymbol{\sigma} \cdot \boldsymbol{n} \cdot (\boldsymbol{\delta} - \boldsymbol{n} \otimes \boldsymbol{n})$.

In the same way, we derive the damage-conjugated thermodynamic force

$$Y_d = \frac{\partial\psi}{\partial d} = \frac{1}{2d^2}\boldsymbol{\epsilon}^c : \mathbb{C}^n : \boldsymbol{\epsilon}^c \tag{9}$$

for a family of closed cracks, and

$$Y_d = \frac{\partial\psi}{\partial d} = \frac{1}{2}\boldsymbol{\sigma} : \mathbb{S}^n : \boldsymbol{\sigma} \tag{10}$$

for a family of open cracks.

2.3 Friction Criterion and Damage Criterion on Crack Scale

Given the local stress $\boldsymbol{\sigma}^c$, it is natural and rational to define for a family of closed cracks a friction criterion in terms of the

normal and shear stress components σ_n^c and $\boldsymbol{\tau}^c$. The following Coulomb-type criterion formulated on the microscale

$$f(\boldsymbol{\sigma}^c) = \|\boldsymbol{\tau}^c\| + \alpha\sigma_n^c \leq 0 \tag{11}$$

is used to characterize the friction-induced inelastic deformation, where α represents the apparent friction coefficient of crack surfaces with asperities.

In continuum damage mechanics, the strain energy release rate-based damage criteria have been widely used, which take the following general form

$$g(Y_d, d) = Y_d - \mathcal{R}(d) \leq 0. \tag{12}$$

Function $\mathcal{R}(d)$ represents the current material resistance to further damage evolution by crack growth.

3 Failure Criterion in the Mohr Plane

3.1 Derivation of the Failure Functions

For open cracks, recall that the local damage criterion is given by

$$g(\boldsymbol{\sigma}, d) = \frac{1}{2}\boldsymbol{\sigma} : \mathbb{S}^n : \boldsymbol{\sigma} - \mathcal{R}(d) \leq 0 \tag{13}$$

By denoting $\kappa = c_t/(2c_n) = 1 - \frac{\nu}{2}$ and $\tau = \|\boldsymbol{\tau}\|$, the damage criterion is cast into the form

$$g(\boldsymbol{\sigma}, d) = \frac{\tau^2}{\kappa} + \sigma_n^2 - 2c_n\mathcal{R}(d) = 0 \tag{14}$$

It is seen that material failure will take place once $\mathcal{R}(d)$ reaches its maximal value at a critical damage $d = d_c$. By defining the uniaxial tensile strength $\sigma_t = \sqrt{2c_n\mathcal{R}(d_c)}$, the following failure function is finally achieved for both the tensile mode ($\tau = 0$) and the tensile-shear mode

$$g(\boldsymbol{\sigma}) = \frac{\tau^2}{\kappa} + \sigma_n^2 - \sigma_t^2 = 0 \tag{15}$$

Under compressive stresses with the algebraic sequence of the principal stresses $\sigma_1 < \sigma_2 < \sigma_3$, it is known a priori that the normal $\boldsymbol{n}$ of the critical cracking plane is located inside the plane $(\boldsymbol{e}_1, \boldsymbol{e}_3)$ (see Fig. 1). For this reason, the stress tensor is written in the following form

$$\boldsymbol{\sigma} = \sigma_3\boldsymbol{\delta} + (\sigma_2 - \sigma_3)\boldsymbol{e}_2 \otimes \boldsymbol{e}_2 + (\sigma_1 - \sigma_3)\boldsymbol{e}_1 \otimes \boldsymbol{e}_1. \tag{16}$$

It follows by introducing Eq. (16) into Eq. (8)

$$\sigma_n^c = \sigma_3 + (\sigma_1 - \sigma_3)(\boldsymbol{e}_1 \cdot \boldsymbol{n})^2 - \frac{c_n}{d}\boldsymbol{\epsilon}^c : (\boldsymbol{n} \otimes \boldsymbol{n}) \tag{17}$$

and

$$\boldsymbol{\tau}^c = (\sigma_1 - \sigma_3)(\boldsymbol{e}_1 \cdot \boldsymbol{n})[\boldsymbol{e}_1 - (\boldsymbol{e}_1 \cdot \boldsymbol{n})\boldsymbol{n}] - \frac{c_t}{d}\boldsymbol{\epsilon}^c \cdot \boldsymbol{n} \cdot (\boldsymbol{\delta} - \boldsymbol{n} \otimes \boldsymbol{n}) \tag{18}$$

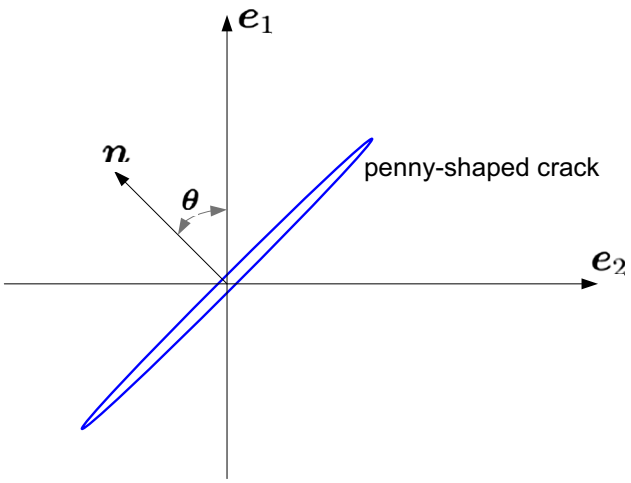

Fig. 1 Illustration of a penny-shaped crack with the normal $\boldsymbol{n}$ inside the plane $(\boldsymbol{e}_1, \boldsymbol{e}_3)$ and forming the angle θ with the axis $\boldsymbol{e}_1$

Further, according to the shear stress vector $\boldsymbol{\tau}$, the flow direction inside the crack plane, denoted by the unit vector $\boldsymbol{t}$, is defined as

$$\boldsymbol{t} = \frac{(\sigma_1 - \sigma_3)(\boldsymbol{e}_1 \cdot \boldsymbol{n})(\boldsymbol{e}_1 - (\boldsymbol{e}_1 \cdot \boldsymbol{n})\boldsymbol{n})}{\|(\sigma_1 - \sigma_3)(\boldsymbol{e}_1 \cdot \boldsymbol{n})(\boldsymbol{e}_1 - (\boldsymbol{e}_1 \cdot \boldsymbol{n})\boldsymbol{n})\|} = \text{sign}(\sigma_1 - \sigma_3)\frac{\boldsymbol{e}_1 - (\boldsymbol{e}_1 \cdot \boldsymbol{n})\boldsymbol{n}}{\sqrt{1 - (\boldsymbol{e}_1 \cdot \boldsymbol{n})^2}} \tag{19}$$

The norm $\|\boldsymbol{\tau}^c\|$, denoted by τ^c, can then be reformulated in terms of τ

$$\tau^c = \tau - \frac{c_t}{d}\boldsymbol{t} \cdot \boldsymbol{\epsilon}^c \cdot \boldsymbol{n} \tag{20}$$

By defining the flow direction tensor

$$\boldsymbol{D} = \boldsymbol{t} \otimes^s \boldsymbol{n} + \alpha\boldsymbol{n} \otimes \boldsymbol{n}, \text{ or } D_{ij} = \frac{1}{2}\left(n_i t_j + n_j t_i\right) + \alpha n_i n_j \tag{21}$$

The friction criterion is finally rearranged into the form

$$f(\boldsymbol{\sigma}, \boldsymbol{\epsilon}^c, d) = \tau + \alpha\sigma_n - \frac{1}{d}\boldsymbol{D} : \mathbb{C}^n : \boldsymbol{\epsilon}^c \leq 0 \tag{22}$$

The evolution of the inelastic strain is determined by adopting an associated flow rule

$$\dot{\boldsymbol{\epsilon}}^c = \lambda^s\frac{\partial f}{\partial \boldsymbol{\sigma}^c} = \lambda^s\boldsymbol{D} \tag{23}$$

According to Eq. (19), under monotonic loading, $\boldsymbol{D}$ is independent on the stress level. When no rotation of the principal directions occurs, the cumulated inelastic strain $\boldsymbol{\epsilon}^c$ can be simply measured as $\boldsymbol{\epsilon}^c = \Lambda^s\boldsymbol{D}$ with the cumulation $\Lambda^s = \int \lambda^s$ operated over the loading history. It follows

$$f(\boldsymbol{\sigma}, \boldsymbol{\epsilon}^c, d) = \tau + \alpha\sigma_n - \frac{\Lambda^s}{d}\boldsymbol{D} : \mathbb{C}^n : \boldsymbol{D} \leq 0 \tag{24}$$

On the other hand, we rewrite the damage criterion (12) by means of the tensor $\boldsymbol{D}$

$$g = \frac{1}{2}\left(\frac{\Lambda^s}{d}\right)^2 \boldsymbol{D} : \mathbb{C}^n : \boldsymbol{D} - \mathcal{R}(d) \leq 0 \tag{25}$$

When it is satisfied, i.e. $g = 0$, we have the relation

$$\frac{\Lambda^s}{d} = 2\sqrt{\frac{\mathcal{R}(d)}{\xi}} \tag{26}$$

with $\xi = 2\boldsymbol{D} : \mathbb{C}^n : \boldsymbol{D} = 2c_n(\kappa + \alpha^2)$.

The friction criterion is finally written in the form

$$f(\boldsymbol{\sigma}, d) = \tau + \alpha\sigma_n - \sqrt{\mathcal{R}(d)\xi} \leq 0 \tag{27}$$

It is seen from the above friction-damage coupling analyses that friction-induced material hardening/softening is actually controlled by the kinetics of the damage resistance function $\mathcal{R}(d)$. In other words, material failure will take place once $\mathcal{R}(d)$ reaches its maximal value at a critical damage $d = d_c$. By defining the purely shear strength $\sigma_\tau = \sqrt{\mathcal{R}(d_c)\xi} = \sigma_t\sqrt{\kappa + \alpha^2}$, the failure function reads

$$f(\boldsymbol{\sigma}, d_c) = \tau + \alpha\sigma_n - \sigma_\tau = 0 \tag{28}$$

3.2 Comparisons with the Griffith Failure Criterion and its Modified Version

In Fig. 2 are presented and compared the original Griffith failure function and its modified version in the Mohr plane. It is seen that the original Griffith criterion is continuous and smooth but would underestimate material strength in compression regime. McClintock and Walsh (1962) amended this shortcoming by taking into account contact condition on closed frictional cracks under local compressive normal stress. However, this improvement caused the mathematical inconsistency that the two parts of the envelope are tangential to each other only for the particular case where $\alpha = 1$.

In the present work, we have dealt in a consistent and unified framework with the cases of open cracks and closed cracks in order to take into account unilateral effects. The unilateral damage as well as damage-friction coupling analyses result in the failure functions (14) and (28) for open and closed microcracks, respectively. The failure criterion is summarized as follows:

$$\begin{cases} \dfrac{\tau^2}{\kappa} + \sigma_n^2 - \sigma_t^2 = 0, & \sigma_n \geq 0 \\ \tau + \alpha\sigma_n - \sigma_\tau = 0, & \sigma_n \leq 0 \end{cases} \tag{29}$$

In Fig. 3 is presented the present failure criterion in the Mohr plane. The failure envelope consists of two parts: the straight line for closed cracks and the elliptically curved line for open cracks. By combining functions (28) and (14), it is proved

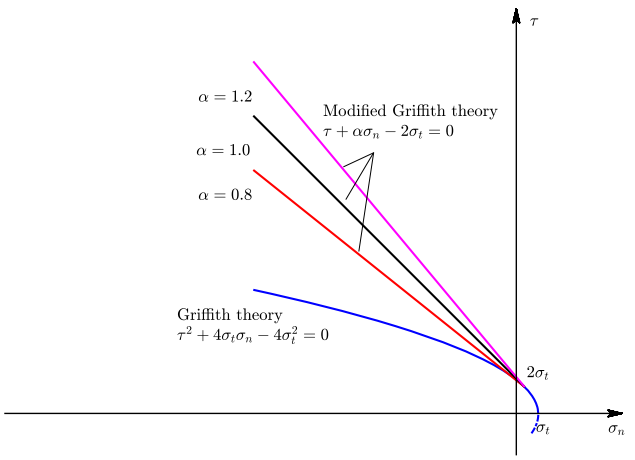

Fig. 2 Illustration of the original Griffith failure criterion and its modification

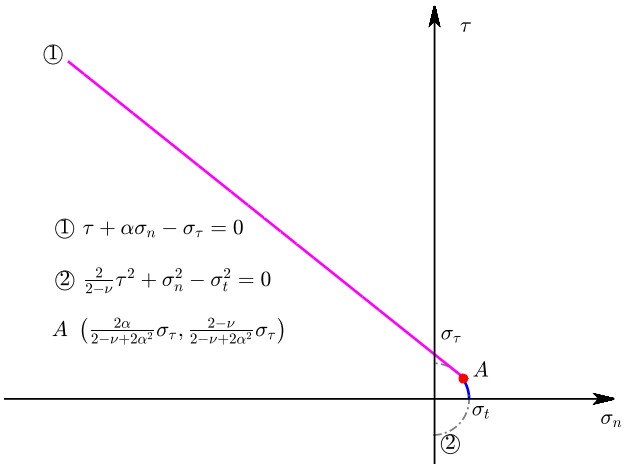

Fig. 3 The new Griffith-type failure envelope (*solid line*) in the Mohr plane

that the two parts are jointed and tangent to each other at point $\left(\frac{\alpha}{\kappa+\alpha^2}\sigma_\tau, \frac{\kappa}{\kappa+\alpha^2}\sigma_\tau\right)$. In other word, they are continuous and smooth in the whole hardening/softening process. Moreover, this $\mathcal{C}_1$-type continuity is independent on the material properties. It is worthy noticing that the derived failure function in compression regime takes the same form as the modification by McClintock and Walsh (1962) to the original Griffith criterion. The difference between them only resides in their intersections with the τ-axis.

4 Failure Criterion in the Plane of Principle Stresses

As aforementioned, brittle rocks usually contain a large number of randomly oriented and distributed microcracks and experience a nonlinear dissipative process by crack

growth, coalescence and localization into a thin band, finally forming a macroscopic shearing plane. Material failure takes place with the occurrence of one or several critical sliding planes inclined at a mathematically determined tip angle. Therefore, in order to derive the failure function, we have to follow such a procedure: find the critical plane and then formulate the failure function. To this end, we distinguish three loading paths usually envisaged in geomechanics.

4.1 Triaxial Tests with Axial Compression

Denoting by θ the angle formed by the axis $\boldsymbol{e}_1$ and the normal $\boldsymbol{n}$ of microcracks in a given family, one has $\boldsymbol{e}_1 \cdot \boldsymbol{n} = \cos\theta$ with $\theta \in \left[0, \frac{\pi}{2}\right]$ (see Fig.1). It follows

$$\tau = \|\boldsymbol{\sigma} \cdot \boldsymbol{n} \cdot (\boldsymbol{\delta} - \boldsymbol{n} \otimes \boldsymbol{n})\| = |\sigma_1 - \sigma_3| \cos\theta \sin\theta \tag{30}$$

and

$$\sigma_n = \boldsymbol{n} \cdot \boldsymbol{\sigma} \cdot \boldsymbol{n} = \sigma_1 \cos^2\theta + \sigma_3 \sin^2\theta \tag{31}$$

Furthermore, triaxial tests with axial compression $(\sigma_1 - \sigma_3 < 0)$ imply

$$\tau = -(\sigma_1 - \sigma_3) \cos\theta \sin\theta \tag{32}$$

By inserting Eq. (31) and Eq. (32) into Eq. (28) and after some arrangements, the friction criterion takes the form

$$f = \sigma_1 - \frac{\cos\theta \sin\theta + \alpha \sin^2\theta}{\cos\theta \sin\theta - \alpha \cos^2\theta}\sigma_3 + \frac{1}{\sin\theta \cos\theta - \alpha \cos^2\theta}\sigma_\tau = 0 \tag{33}$$

It is now convenient to define the orientation-dependent function $h(\theta) = \cos\theta \sin\theta - \alpha \cos^2\theta$. One can prove that the maximal value of $h(\theta)$ is obtained with the critical angle θ_c, which satisfies the following condition

$$\tan\theta_c = \sqrt{\alpha^2 + 1} + \alpha \tag{34}$$

Frictional sliding along the critical plane inclined at $\theta = \theta_c$ leads to the macroscopic failure of the material. Substitution of Eq. (34) into Eq. (33) gives

$$f(\sigma_1, \sigma_3) = \sigma_1 - \tan^2\theta_c \sigma_3 + 2\tan\theta_c \sigma_\tau = 0 \tag{35}$$

Let us define the uniaxial compressive strength σ_c by setting $\sigma_2 = \sigma_3 = 0$

$$\sigma_c = 2\tan\theta_c \sigma_\tau = 2\tan\theta_c \sqrt{\mathcal{R}(d_c)\xi} \tag{36}$$

The failure function is written in the following final form

$$f(\sigma_1, \sigma_3) = \sigma_1 - \tan^2\theta_c \sigma_3 + \sigma_c = 0 \tag{37}$$

Moreover, the friction coefficient α can be related to a friction angle ϕ such that $\alpha = \tan\phi$. It is further shown that there exists the following relation between the two angles ϕ and θ_c

$$\theta_c = \frac{\pi}{4} + \frac{\phi}{2}. \tag{38}$$

The above trans-scale relationship allows the parameter α to be determined from a series of triaxial compression tests.

4.2 Triaxial Tests with Axial Extension

In this loading case, the norm of the shear stress vector τ is expressed as

$$\tau = (\sigma_1 - \sigma_3) \cos\theta \sin\theta \tag{39}$$

This time, the friction criterion (28) is reformulated as follows

$$f = \sigma_1 - \frac{\cos\theta \sin\theta - \alpha \sin^2\theta}{\cos\theta \sin\theta + \alpha \cos^2\theta}\sigma_3 - \frac{1}{\sin\theta \cos\theta + \alpha \cos^2\theta}\sigma_\tau = 0 \tag{40}$$

We now define $h(\theta) = \cos\theta \sin\theta + \alpha \cos^2\theta$. It is proved that the maximal value of $h(\theta)$ is obtained at $\theta = \theta_e$ which satisfies the condition

$$\tan\theta_e = \sqrt{\alpha^2 + 1} - \alpha \tag{41}$$

The failure criterion takes the expression

$$f(\sigma_1, \sigma_3) = \sigma_1 - \tan^2\theta_e \sigma_3 - \sigma_e = 0 \tag{42}$$

with the axial extension strength $\sigma_e = 2\tan\theta_e \sigma_\tau$ and the ratios $\sigma_c/\sigma_e = \tan^2\theta_c$ and $\sigma_e/\sigma_c = \tan^2\theta_e$.

Similarly, the following relation between ϕ and θ_e is achieved

$$\theta_e = \frac{\pi}{4} - \frac{\phi}{2} \tag{43}$$

4.3 Tensile Failure

We now proceed to reformulate the tensile failure function (14) in terms of the principal stresses. By combining Eqs. (14), (30) and (31), the damage criterion for open tensile cracks is rewritten in the form

$$g = \frac{1}{\kappa}(\sigma_1 - \sigma_3)^2 \cos^2\theta \sin^2\theta + \left[\sigma_3 + (\sigma_1 - \sigma_3)\cos^2\theta\right]^2 - \sigma_t^2 = 0 \tag{44}$$

Accordingly, we define the following orientation-dependent function

$$h(\theta) = \frac{1}{\kappa}(\sigma_1 - \sigma_3)^2 \cos^2\theta \sin^2\theta + \left(\sigma_1 \cos^2\theta + \sigma_3 \sin^2\theta\right)^2 \tag{45}$$

In order to derive the critical failure plane, we impose the condition

$$\frac{\mathrm{dh}}{\mathrm{d}\theta} = \frac{1}{2\kappa}(\sigma_1 - \sigma_3)^2 \sin 2\theta \cos 2\theta - \left(\sigma_1 \cos^2\theta + \sigma_3 \sin^2\theta\right) (\sigma_1 - \sigma_3) \sin 2\theta = 0 \tag{46}$$

leading to two candidates of solution

$$\sin 2\theta = 0 \tag{47}$$

and

$$\frac{1}{2\kappa}(\sigma_1 - \sigma_3)\cos 2\theta - \left(\sigma_1 \cos^2\theta + \sigma_3 \sin^2\theta\right) = 0 \tag{48}$$

The latter one can be cast into the form

$$\tan^2\theta = \frac{(1-2\kappa)\sigma_1 - \sigma_3}{\sigma_1 - (1-2\kappa)\sigma_3} \tag{49}$$

or for latter reference

$$\cos^2\theta = \frac{\sigma_1 - (1-2\kappa)\sigma_3}{2(1-\kappa)(\sigma_1 - \sigma_3)}, \quad \sin^2\theta = \frac{(1-2\kappa)\sigma_1 - \sigma_3}{2(1-\kappa)(\sigma_1 - \sigma_3)} \tag{50}$$

On the other hand, for open tensile cracks, when neglecting the initial opening degree, the opening-closure transition imposes the condition $\sigma_n \geq 0$ for open cracks. More explicitly, one has

$$\sigma_1 \cos^2\theta + \sigma_3 \sin^2\theta \geq 0 \tag{51}$$

We now distinguish the following cases:

- *Case 1* $\sigma_1 > 0$ and $\sigma_3 = 0$. Eq. (49) gives the relation $\tan^2\theta = 1 - 2\kappa = -1 + \nu < 0$, which is thus impossible. We must have $\sin 2\theta = 0$, leading to the solutions $\theta = 0$ or $\theta = \frac{\pi}{2}$ and the former giving a bigger value for $h(\theta)$. The failure function then takes the form

  $$\sigma_1 - \sigma_t = 0 \tag{52}$$

  corresponding to a purely tensile failure.
- *Case 2* $\sigma_3 > 0$ and $\sigma_1 = 0$. Eq. (49) becomes $\tan^2\theta = \frac{1}{1-2\kappa}$, which is also impossible. In this case, the solution will be $\theta = \frac{\pi}{2}$ and the tensile failure function is obtained

  $$\sigma_3 - \sigma_t = 0 \tag{53}$$

- *Case 3* $\sigma_1 > 0$ and $\sigma_3 < 0$, that gives $\sigma_1 - \sigma_3 > 0$. According to Eq. (50), one has $(1-2\kappa)\sigma_3 \leq \sigma_1 \leq \frac{\sigma_3}{1-2\kappa}$; on the other hand, combination of Eq. (49) with condition (51) gives $\sigma_1 + \sigma_3 \geq 0$. On summary, the stresses are constrained by the following condition

  $$-\sigma_1 \leq \sigma_3 \leq (1-2\kappa)\sigma_1 \tag{54}$$

  It is shown that the failure function takes the following form (see "Appendix 1" for the proof)

  $$\frac{1}{4(1-\kappa)}(\sigma_1 + \sigma_3)^2 + \frac{1}{4\kappa}(\sigma_1 - \sigma_3)^2 - \sigma_t^2 = 0 \tag{55}$$

  corresponding to a tensile-shear failure mode.
  Complementary to Case 3 when $(1-2\kappa)\sigma_1 \leq \sigma_3 < 0$, we must have the condition $\sin 2\theta = 0$ and the solution $\theta = 0$ is attained according to function (44).
- *Case 4* $\sigma_1 < 0$ and $\sigma_3 > 0$, that gives $\sigma_1 - \sigma_3 < 0$. We then derive from Eq. (50) the relation $(1-2\kappa)\sigma_3 \geq \sigma_1 \geq \frac{\sigma_3}{1-2\kappa}$ and $\sigma_1 + \sigma_3 \geq 0$ by combining (49) and (51), leading to the inequality

  $$-\sigma_3 \leq \sigma_1 \leq (1-2\kappa)\sigma_3 \tag{56}$$

  In this case, the failure function (55) is shared.
  Complementary to Case 4 when $(1-2\kappa)\sigma_3 \leq \sigma_1 < 0$. One shall take the candidate $\sin 2\theta = 0$. According to function (44), we finally have the solution $\theta = \frac{\pi}{2}$ and $\sigma_3 = \sigma_t$.
- *Case 5* $\sigma_1 > 0$ and $\sigma_3 > 0$. There is no solution for the candidate (49). We must have $\sin 2\theta = 0$. More precisely, $\theta = 0$ for $\sigma_1 > \sigma_3$ or $\theta = \frac{\pi}{2}$ for $\sigma_1 < \sigma_3$.

4.4 Summary on the Failure Functions

It is now our purpose to formulate the complete failure function based on the above detailed analyses. We are particularly concerned with the loading path of triaxial compression. By collecting the failure functions achieved in the previous parts, one has

$$\begin{cases} \sigma_3 - \sigma_t = 0, & \text{if } -(1-\nu)\sigma_t \leq \sigma_1 \leq 0 \\ \frac{1}{\nu}(\sigma_1 + \sigma_3)^2 + \frac{1}{2-\nu}(\sigma_1 - \sigma_3)^2 - 2\sigma_t^2 = 0, & \text{if } -\sigma_3 \leq \sigma_1 \leq -(1-\nu)\sigma_t \\ \sigma_1 - \tan^2\theta_c \sigma_3 + \sigma_c = 0, & \text{if } \sigma_1 \leq -\sigma_3 \end{cases} \tag{57}$$

It is worth indicating that unlike the original Griffith failure function that contains two parts, the present failure criterion consists of three parts, corresponding to three failure modes of brittle rocks: purely tensile failure, tensile-shear failure and compressive-shear failure.

4.5 Some Discussions on the New Failure Criterion

Based on the above analyses, the complete failure envelope in the (σ_3, σ_1) plane is depicted in Fig. 4, from which are captured the following features:

- The whole failure envelope is symmetric with respect to the straight line defined by $\sigma_1 - \sigma_3 = 0$, the upper and lower branches corresponding to the extension and compression loading paths, respectively. Moreover, each branch contains three parts: a cutoff part, an elliptically curved line defined by Eq. (55) which describes the tensile-shear failure for the case of open cracks, and the second straight line (Eq. (37) or Eq. (42)) which reflects the compressive-shear failure for the case of closed cracks under compressive normal stress. The smooth transition from the tensile failure mode to compressive-shear failure mode can be demonstrated theoretically (see "Appendix 2").
- The two straight lines are tangent to the elliptical curve, respectively, at point $A(\sigma_t, (1-2\kappa)\sigma_t)$ and point

$$B\left(\frac{1+2(\kappa-1)\cos^2\theta_c}{1+4(\kappa-1)\sin^2\theta_c\cos^2\theta_c}\sigma_c\cos^2\theta_c,\right.$$
$$\left.-\frac{1+2(\kappa-1)\sin^2\theta_c}{1+4(\kappa-1)\cos^2\theta_c\sin^2\theta_c}\sigma_c\cos^2\theta_c\right),$$

as proved in "Appendix 2" and illustrated in the amplification region of Fig. 4, which presents an appealing feature of continuity and smoothness of the new failure criterion.

- The compressive strength σ_c and the tensile strength σ_t are not symmetrical. It is not surprising in view that the unilateral contact effect has been taken into account properly. Moreover, unlike the Griffith criterion, the ratio σ_c/σ_t is here not fixed but varies with the material properties. More precisely, one has

$$\frac{\sigma_c}{\sigma_t} = 2\left(\sqrt{\alpha^2+1}+\alpha\right)\sqrt{1-\frac{\nu}{2}+\alpha^2} = 2\tan\theta_c\sqrt{1-\frac{\nu}{2}+\alpha^2} \tag{58}$$

The evolution of the ratio σ_c/σ_t with the friction coefficient is presented in Fig. 5. It is seen that a bigger value of friction coefficient leads to a higher level of a compressive to tensile strength ratio, which is obviously consistent with laboratory observations.

- It is noted that on the basis of stress analyses within the framework of fracture mechanics Ashby and Sammis (1990) proposed a crack initiation condition and final failure criterion for brittle rocks in compression. The tensile failure mode as well as the transitional failure mode were not addressed. It is also interesting to notice that the new criterion (37), the modified part by McClintock and Walsh (1962) to the original Griffith criterion, and the criterion proposed by Ashby and Sammis (1990) all take a linear form in compression regime. To a certain extent, their comparisons allow to justify the use of an apparent (effective) friction coefficient in the present work.

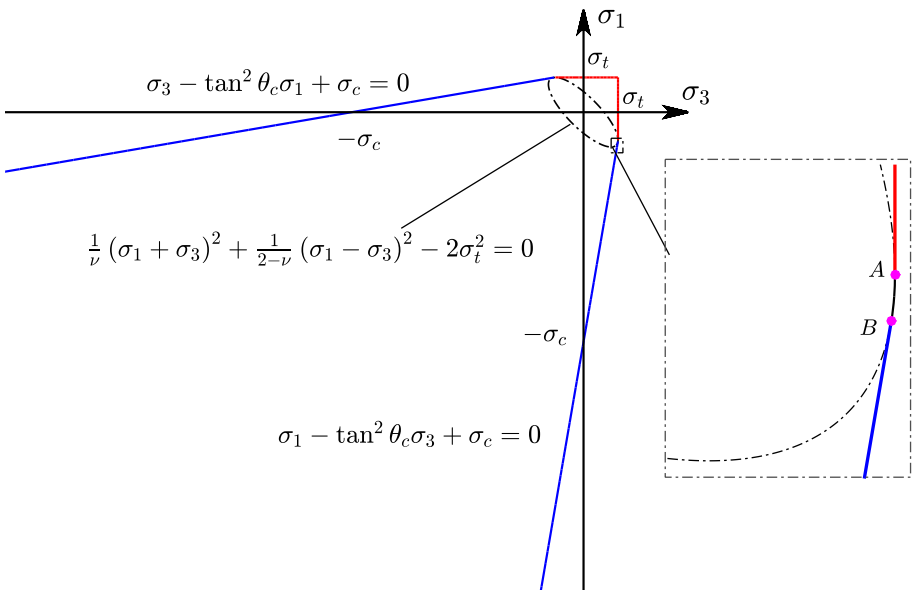

Fig. 4 The new strength envelope (*solid line*) in the plane (σ_3, σ_1) with point A and point B

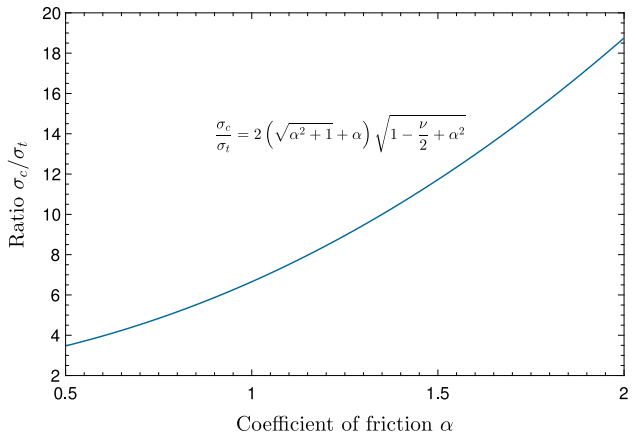

Fig. 5 Variation of the ratio of compressive strength to tensile strength at $\nu = 0.2$

5 Comparisons with Experimental Data for Typical Brittle Rocks

This section is concerned with the evaluation on the derived failure criterion by comparison with experimental data from triaxial compression tests on typical brittle rocks. The calibration procedure is as follows: calibrate first the two parameters α and $\mathcal{R}(d_c)$ of the compressive failure function because triaxial compression tests are more easily performed to obtain reliable data with respect to tensile tests; next, predict the tensile strength σ_t according to the ratio (58); finally, plot the whole strength envelope and compare it with experimental failure data. It is worthy emphasizing that complete and consistent testing data including the zone of tensile failure were rarely reported in literatures.

5.1 Westerly Granite

We focus first on the strength feature of Westerly granite (Haimson and Chang 2000; Hopkins 1986) because of its relatively complete loading range. According to experimental data, the failure stresses for lower and moderate levels of confining pressures can be fitted quite well by the linear function $\sigma_1 = 11.11\sigma_3 + 199.6$, its comparison with function (37) leading to the relations: $\tan^2\theta_c = 11.11$ and $\sigma_c = 2\tan\theta_c\sqrt{\mathcal{R}(d_c)\xi} = 199.6$ MPa. From the former is determined the apparent friction coefficient $\alpha = 1.52$, and then according to Eq. (58) the tensile strength $\sigma_t = 16.6$ MPa is predicted for a typical value of $\nu = 0.2$.

Figure 6 compares theoretical prediction and experimental data. The predicted tensile strength, although smaller than the value of 17.9 MPa from isotropic analyses (Zhu 2016), is still 30 % bigger than the testing data 12.5 MPa. This difference should be caused by the neglect of initial opening of micro-defects. As one of the

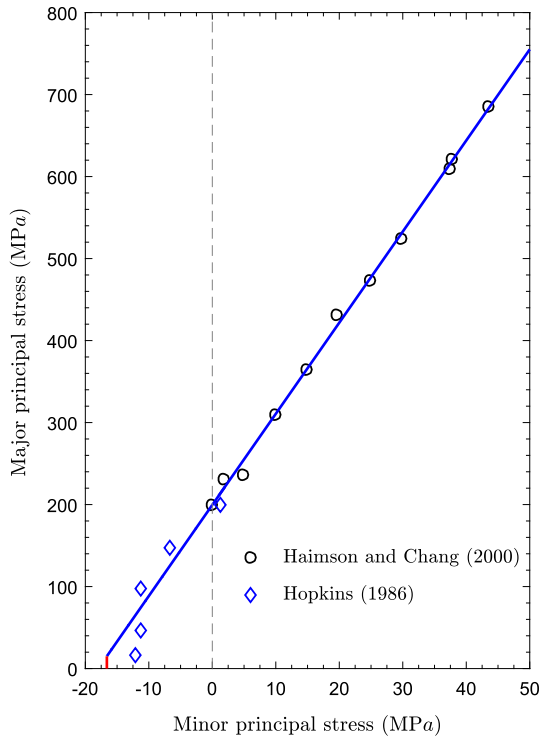

Fig. 6 Validation of the proposed failure criterion with Westerly granite

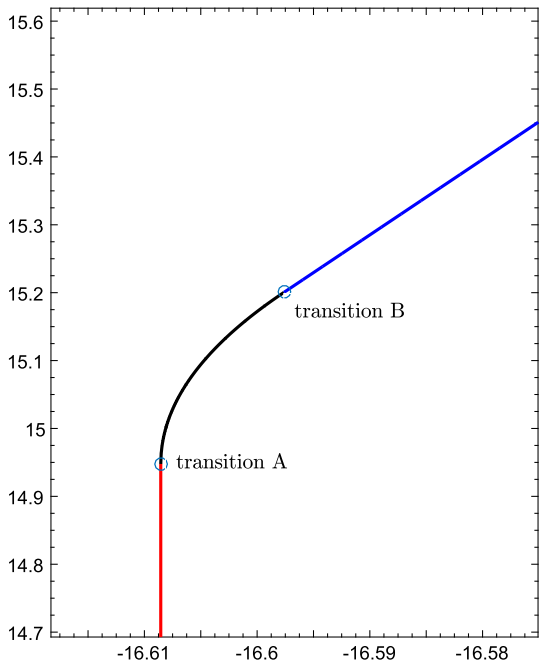

Fig. 7 Local amplification of Fig. 6 to show the smooth transition between the different failure modes

experimental evidences, in the first phase of a triaxial compression test with low or moderate confining pressure, the stress–strain curve of brittle rocks is generally concave due to the progressive closure of existing microcracks. In

this view, further improvement can be expected by accounting for the effect of progressive closure of initial cracks.

In order to show the transition of the failure modes, we choose to amplify the transition zone, as shown in Fig. 7. It is seen that the extent of the zone between points A and B denoting the hybrid tensile-shear failure mode is very limited. That is why smooth transition from one failure mode to another is generally very difficult to be clearly identified in experiment. As an exception, the laboratory tests conducted by Ramsey and Chester (2004) on dog-bone samples of Carrara marble gained a great success and opened a new way to achieve complete failure information on rock strength.

5.2 Lac du Bonnet Granite

By following the same procedure, we now perform the comparison between theoretical prediction and experimental data on the failure stresses of Lac du Bonnet granite. For that, use has been made of the testing data appeared in Carter et al. (1991). The two basic strength parameters α and $\mathcal{R}(d_c)$ are determined by fitting the experimental data for low and moderate confining pressures. The fitting line takes the function $\sigma_1 = 14.3\sigma_3 + 230.3$, giving the apparent friction coefficient $\alpha = 1.76$, the compressive strength $\sigma_c = 230.3$ MPa and the tensile strength $\sigma_t = 15.23$ MPa. The predicted strength envelope and the locally amplified transition zone

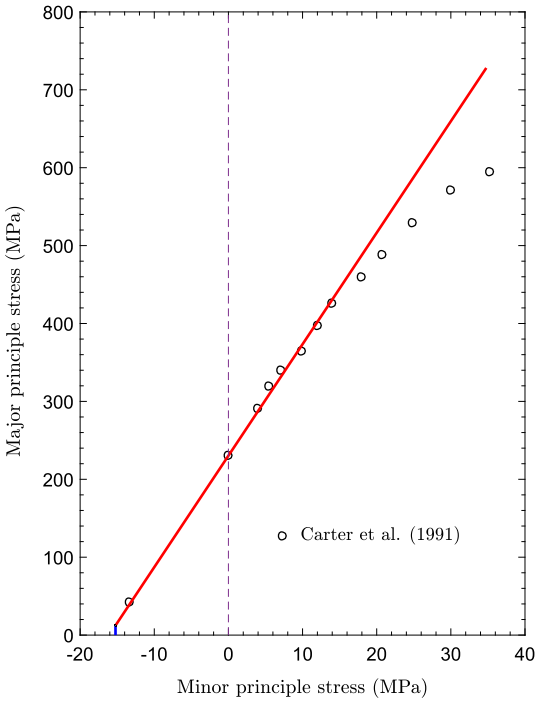

Fig. 8 Comparison of theoretical prediction with experimental data from triaxial compression tests on Lac du Bonnet granite

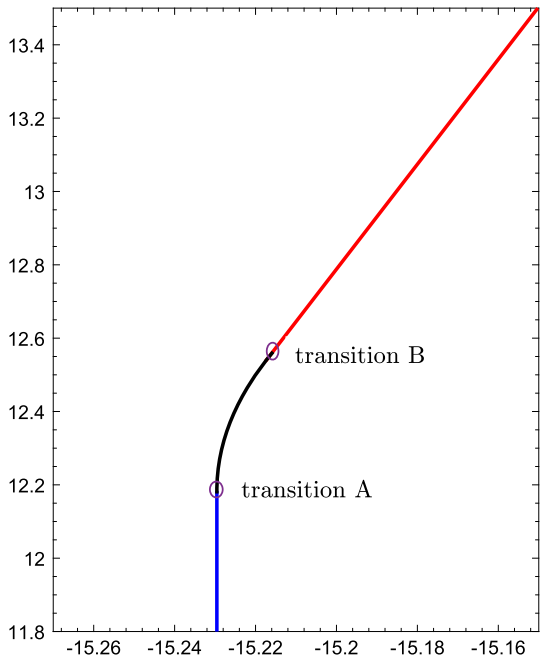

Fig. 9 Local amplification of Fig. 8 to show the smooth transition between the different failure modes

are plotted in Figs. 8 and 9, respectively. Globally, the comparisons and comments made on Westerly granite are shared by Lac du Bonnet granite. Just like the modified Griffith failure criterion and the criterion proposed by Ashby and Sammis (1990), the proposed failure function cannot predict satisfactorily the failure of crystalline rocks under high confining pressures, in which some ductile failure mechanisms may be involved but have not been taken into account in the present model.

6 Concluding Remarks

We proposed a new way to derive a mechanisms-based failure criterion for brittle rocks weakened by penny-shaped microcracks. Inherent combination of strength prediction with inelastic deformation analyses makes it thoroughly different from the existing ones. The closed-form failure functions corresponding to the different failure modes have been determined using an upscaling method. The strength envelope possesses the $\mathcal{C}_1$-type continuity, which is independent on material properties and state variables. As one of the original contributions, the hybrid fracture and the smooth transition from tensile fracture to compressive-shear fracture have been demonstrated theoretically. More useful remarks are made as follows:

In the presented framework, theoretical derivation of failure criterion has been regarded as one of mandatory parts of developing a complete multiscale constitutive

model for cracked rocks. In other words, the criterion we established is the natural result of a set of constitutive equations (e.g., damage and friction criteria, evolution laws of internal variables) but not the starting point to formulate such equations by incorporating evolutions laws as well as hardening/softening functions.

The failure mechanisms behind theoretical derivations are quite clear. The formulations involve two crack geometric states (open or closed), two nonlinear dissipation mechanisms (anisotropic unilateral damage by cracking and inelastic deformation by frictional sliding) and three brittle failure modes (purely tensile mode, tensile-shear model and compressive-shear mode). To the author's knowledge, failure criteria with these salient features have not ever been reported in literatures.

The present contribution amends the original Griffith failure criterion by taking into account the effect of friction on closed cracks under normal compressive stress, and simultaneously improves the modified Griffith criterion in the sense that the new one ensures theoretically the smoothness at the transition of the different failure modes.

Up to now, the effect of the intermediate principal stress remains a theoretical issue largely open to the scientific community and is also beyond the scope of the present work. In both the damage driving force (10) for open cracks and the friction criterion (11) for closed cracks are involved two stress-fabric invariants: $\boldsymbol{\sigma} : \mathbb{T} : \boldsymbol{\sigma}$ and $\boldsymbol{\sigma} : \mathbb{N} : \boldsymbol{\sigma}$. However, the fourth-order orientation-dependent tensors $\mathbb{T}$ and $\mathbb{N}$ do not provide a closed-form decomposition of the fourth-order identity tensor $\mathbb{I}$. Incorporation of the invariant $\boldsymbol{\sigma} : (\mathbb{I} - \mathbb{N} - \mathbb{T}) : \boldsymbol{\sigma}$ into the constitutive model may cast a new light on the investigation on the effect of the intermediate principal stress.

Future work along this line may include first the account of pore pressure effect on material strength. On this topic, some preliminary results have been achieved under isotropic simplification for both the damage and inelastic strain (Zhu 2016). Moreover, according to experimental results, the ratio of compressive strength to tensile strength may vary within a large range (Hoek and Martin 2014). For some rocks, prediction by Eq. (58) may underestimate this ratio. This could be partially caused by the neglect of initial crack opening in the disturbed samples. In the present model, according to the opening/closure transition condition of microcracks, tensile failure only occurs for open cracks and has to be triggered by applying a macroscopic tensile stress. Thus, further efforts can be made by taking into account an initial normal strain.

Acknowledgments This work has been jointly supported by the National Natural Science Foundation of China (Grant Nos. 11202063 and 51679068), the Fundamental Research Funds for the Central Universities (Grant Nos. 2014B06914 and 2016B20214) and the 111 Project (Grant No. B13024).

Appendix 1: Derivation of Function (55)

According to the condition (54) and Eq. (49), we derive the range of the dip angle as $0 \leq \theta \leq \frac{\pi}{4}$. On the one hand, by combining Eq. (51) and the conditions that $\sigma_1 > 0$ and $\sigma_3 < 0$, from Eq. (47) is derived the potential solution $\theta_1 = 0$. On the other hand, introduction of Eq. (50) into Eq. (44) gives

$$h(\theta_2) = \frac{1}{4(1-\kappa)}(\sigma_1 + \sigma_3)^2 + \frac{1}{4\kappa}(\sigma_1 - \sigma_3)^2 \tag{59}$$

for the value of θ determined by Eq. (50).

Next, we make a difference between $h(\theta_2)$ and $h(\theta_1) = \sigma_1^2$

$$h(\theta_2) - h(\theta_1) = \frac{1}{4\kappa(1-\kappa)}[(1-2\kappa)\sigma_1 - \sigma_3]^2 \geq 0 \tag{60}$$

and also the difference between $h(\theta_2)$ and $h\left(\theta = \frac{\pi}{4}\right) = \frac{1}{4\kappa}(\sigma_1 - \sigma_3)^2 + \frac{1}{4}(\sigma_1 + \sigma_3)^2$

$$h(\theta_2) - h\left(\frac{\pi}{4}\right) = \frac{1}{4}\frac{\kappa}{1-\kappa}(\sigma_1 + \sigma_3)^2 \geq 0 \tag{61}$$

As an inclusion, under the conditions that $\sigma_1 > 0$ and $\sigma_3 < 0$, the solution given by Eq. (50) leads to a maximal value of $h(\theta)$. Accordingly, the failure function takes the form

$$g(\sigma_1, \sigma_3) = \frac{1}{4(1-\kappa)}(\sigma_1 + \sigma_3)^2 + \frac{1}{4\kappa}(\sigma_1 - \sigma_3)^2 - \sigma_t^2 = 0 \tag{62}$$

By following the same procedure, we can derive the same failure function for the case that $\sigma_1 < 0$ and $\sigma_3 > 0$.

Appendix 2: Proof of the Continuity and Smoothness of the Failure Envelope

It is proposed to reformulate Eq. (62) in the following form

$$g(\sigma_1, \sigma_3) = \sigma_1^2 + \sigma_3^2 - 2(1-2\kappa)\sigma_1\sigma_3 - 4\kappa(1-\kappa)\sigma_t^2 = 0 \tag{63}$$

In order to prove the continuity and smoothness at point A, we set $\sigma_3 = \sigma_t$ in Eq. (63),

$$[\sigma_1 - (1-2\kappa)\sigma_t]^2 = 0 \tag{64}$$

leading to the unique solution $\sigma_1 = (1-2\kappa)\sigma_t$. In other words, the point A takes the coordinate $(\sigma_t, (1-2\kappa)\sigma_t)$.

As for the point B, from Eq. (37) is derived

$$\sigma_1 = \tan^2\theta_c\sigma_3 - \sigma_c \tag{65}$$

By combining Eq. (63) and Eq. (65), we obtain the following quadratic function in terms of σ_3

$$a\sigma_3^2 + b\sigma_3 + c = 0 \tag{66}$$

with the coefficients

$$a = \left(\tan^2\theta_c + 1\right)^2 + 4(\kappa-1)\tan^2\theta_c \tag{67}$$

$$b = 2\left[-\tan^2\theta_c + (1-2\kappa)\right]\sigma_c \tag{68}$$

$$c = \sigma_c^2 - 4\kappa(1-\kappa)\sigma_t^2 \tag{69}$$

It is proved that

$$\begin{aligned}\triangle &= b^2 - 4ac \\ &= 4\kappa(1-\kappa)\left[-4\tan^2\theta_c\alpha^2 + \left(\tan^2\theta_c - 1\right)^2\right]\sigma_t^2\end{aligned} \tag{70}$$

Further, from Eq. (34) is derived the relation

$$\alpha = \frac{1}{2}\left(\tan\theta_c - \frac{1}{\tan\theta_c}\right) \tag{71}$$

Its insertion into Eq. (70) provides $\Delta = 0$, implying that function (66) has one unique solution

$$\sigma_3 = -\frac{b}{2a} = \frac{1 + 2(\kappa-1)\cos^2\theta_c}{1 + 4(\kappa-1)\sin^2\theta_c\cos^2\theta_c}\sigma_c\cos^2\theta_c \tag{72}$$

It follows

$$\sigma_1 = -\frac{1 + 2(\kappa-1)\sin^2\theta_c}{1 + 4(\kappa-1)\cos^2\theta_c\sin^2\theta_c}\sigma_c\cos^2\theta_c \tag{73}$$

References

Ashby MF, Sammis CG (1990) The damage mechanics of brittle solids in compression. Pure Appl Geophys 133(3):489–521

Benveniste Y (1986) On the Mori-Tanaka method in cracked bodies. Mech Res Comm 13(4):193–201

Brace WF (1960) An extension of the Griffith theory of fracture to rocks. J Geophys Res 65(10):3477–3480

Brace WF, Bombolakis E (1963) A note on brittle crack growth in compression. J Geophys Res 68(12):3709–3713

Carter BJ, Duncan EJS, Lajtai EZ (1991) Fitting strength criteria to intact rock. Geotech Geol Eng 9(9):73–81

Clausing DP (1959) Comparison of Griffith's theory with Mohr's failure criteria. In: The 3rd US symposium on rock mechanics (USRMS), Golden

Drucker DC, Prager W (1952) Soil mechanics and plastic analysis for limit design. Q Appl Math 10(2):157–165

Griffith AA (1921) The phenomena of rupture and flow in solids. Philos Trans R Soc Lond (Ser A) 22:163–198

Griffith AA (1924) Theory of rupture. In: Proceedings of the 1st international congress of applied mechanics. Delft, Tech. Boekhandel en Drukkerij J Walter Jr, pp 55–63

Haimson B, Chang C (2000) A new true triaxial cell for testing mechanical properties of rock and its use to determine rock strength and deformability of Westerly granite. Int J Rock Mech Min Sci 37:285–296

Hatzitrifon NK, Gdoutos EE (1988) On the Griffith criterion for three-dimensional cracks. Int J Eng Sci 26:833–836

Hoek ET, Bieniawski Z (1965) Brittle fracture propagation in rock under compression. Int J Fract 1(3):137–155

Hoek ET, Brown E (1980) Empirical strength criterion for rock masses. J Geotech Eng ASCE 106(GT9):1013–1035

Hoek ET, Martin CD (2014) Fracture initiation and propagation in intact rock—a review. J Rock Mech Geotech Eng 6:287–300

Hopkins TW (1986) Microfracturing in Westerly granite experimentally extended wet and dry at temperature to 800°C and pressure to 200 MPa. M.Sc. Thesis, Texas A&M University

Kassir MK, Sih GC (1967) Griffith's theory of brittle fracture in three dimensions. Int J Eng Sci 5(12):899–918

Kachanov M (1992) Effective elastic properties of cracked solid: critical review of some basic concepts. App Mech Rev ASME 45(8):304–335

Keer LM (1966) A note on shear and combined loading for a penny-shaped cracks. J Mech Phy Solids 14:1–6

Margolin LG (1984) A generalized Griffith criterion for crack propagation. Eng Fract Mech 19(3):539–543

McClintock FA, Walsh B (1962) Friction on Griffith cracks in rocks under pressure. In: Proceedings of the 4th U.S. national congress of applied mechanics, pp 1015–1021

Mori T, Tanaka T (1973) Averages stress in matrix and average elastic energy of materials with misfitting inclusions. Acta Metall 21:571–74

Patersson MS, Wong TF (2010) Griffith theory of brittle failure. Chapter 4 in Experimental rock deformation—the brittle field. Springer, Berlin

Pensée V, Kondo D, Dormieux L (2002) Micromechanical analysis of anisotropic damage in brittle materials. J Eng Mech ASCE 128(8):889–897

Ramsey JM, Chester FM (2004) Hybrid fracture and the transition from extension fracture to shear fracture. Nature 428(6978):63–66

Sack RA (1946) Extension of Griffith's theory of rupture to three dimensions. Proc Phys Soc 58(6):729–736

Wang EZ, Shrive NG (1993) On the Griffith criteria for brittle fracture in compression. Eng Fract Mech 46(1):15–26

Zhu QZ, Kondo D, Shao JF (2008a) Micromechanical analysis of coupling between anisotropic damage and friction in quasi brittle materials: role of the homogenization scheme. Int J Solids Struct 45(5):1385–1405

Zhu QZ, Kondo D, Shao JF, Pensée V (2008b) Micromechanical modelling of anisotropic damage in brittle rocks and application. Int J Rock Mech Min Sci 45:467–477

Zhu QZ, Shao JF (2015) A refined micromechanical damage-friction model with strength prediction for rock-like materials under compression. Int J Solids Struct 60–61:75–83

Zhu QZ (2016) Strength prediction of dry and saturated brittle rocks by unilateral damage-friction coupling analyses. Comput Geotech 73:16–23

Zhu QZ, Zhao LY, Shao JF (2016) Analytical and numerical analysis of frictional damage in quasi brittle materials. J Mech Phys Solids 92:137–163